Research Square

Preprints are preliminary reports that have not undergone peer review.
They should not be considered conclusive, used to inform clinical practice,
or referenced by the media as validated information.

Dual-functional biomass-based graphene aerogel derived from the Tibetan medicinal plant Pedicularis kansuensis for synergistic removal of antibiotic resistance genes in swine wastewater

Shuai Liu
Xinjiang Agricultural University
Fang Wang
Xinjiang Agricultural University
Mo Chen
Xinjiang Agricultural University
YaXing Wu
Xinjiang Agricultural University
Jing Deng
Xinjiang Agricultural University
Adila Mamatrozi
Xinjiang Agricultural University
Shanshan Wang
SSWang0825@163.com
Xinjiang Agricultural University
Hongtao Jia
Xinjiang Agricultural University

Article

Keywords: Pedicularis kansuensis, Graphene aerogel, ARGs, Swine wastewater, Bacterial community

Posted Date: July 14th, 2026

DOI: https://doi.org/10.21203/rs.3.rs-10252071/v1

License: This work is licensed under a Creative Commons Attribution 4.0 International License.
Read Full License

Additional Declarations: No competing interests reported.

Abstract

The proliferation of antibiotic resistance genes (ARGs) in livestock wastewater poses an escalating threat to ecological safety and public health. Conventional treatment technologies, including biochar adsorption and advanced oxidation, suffer from limitations such as secondary pollution, low recovery, and unclear degradation mechanisms. In this study, a novel biomass-based graphene aerogel (PKGA) was fabricated via a mild hydrothermal self-assembly approach (95°C) using the invasive Tibetan medicinal plant *Pedicularis kansuensis* Maxim. as the biomass precursor. The mild synthesis condition successfully preserved the bioactive secondary metabolites (alkaloids, flavonoids, and phenylethanoid glycosides) of *Pedicularis kansuensis*, endowing PKGA with intrinsic antibacterial activity in addition to its physical adsorption capacity. PKGA was applied to treat real swine wastewater at dosages of 5, 20, and 50 mg/100 mL. Results showed that PKGA significantly reduced chemical oxygen demand (COD), total nitrogen, and total phosphorus in a dose-dependent manner, while simultaneously decreasing the relative abundances of eleven targeted ARGs (*sul1*, *sul2*, *tetA*, *tetC*, *tetW*, *tetX*, *ermB*, *ermF*, *cmlA1-01*, *cmlA1-02*) and the mobile genetic element intI1. 16S rRNA gene sequencing revealed that PKGA reshaped the bacterial community by suppressing typical ARG-hosting taxa (e.g., *Bacteroides*, *Sedimentibacter*, *Macellibacteroides*) and enriching multifunctional genera such as Pseudomonas. Notably, *Pseudomonas* exhibited a contrasting correlation pattern with different ARGs - positive with sul1 but significantly negative with tetC - revealing a strain-level functional succession from ARG-carrying to non-resistant degradation-capable types. The dual-mechanism removal of ARGs by PKGA, combining graphene-based adsorption and plant-derived biological inhibition, provides an innovative and environmentally friendly strategy for ARG mitigation in livestock wastewater. This study also offers a sustainable utilization pathway for the harmful invasive plant *Pedicularis kansuensis*, achieving the synergy of “ecological remediation by ecological harm”.

1. Introduction

The abuse of antibiotics has caused a long-term impact on the ecological environment, especially the harm caused by antibiotic resistance genes (ARGs), which has received more attention and has become a new type of environmental pollutant in recent years[1]. Antibiotics are mainly used for human disease prevention, poultry and aquaculture disease prevention, and feed additives. Antibiotics can lead to prolonged exposure of organisms to chronic exposure of antibiotics, which can alter the structure and function of microbial communities and induce the generation of ARGs and antibiotic-resistant bacteria (ARB)[2]. For example, a variety of bacteria isolated from the water of an aquaculture farm in Chile were resistant to amoxicillin, erythromycin, ampicillin, and chloramphenicol[3]. Moreover, ARGs may be vertically transmitted to offspring or horizontally transferred between species via mobile genetic elements (MGEs), posing serious threats to ecosystem integrity and human health once acquired by pathogenic bacteria[4–5].

The accumulation of antibiotic residues and the dissemination of ARGs from livestock production have severely constrained the sustainable development of animal husbandry in China. According to national

statistics, approximately 97,000 tons of antibiotics were used in animal husbandry in China in 2015, accounting for 46.1% of the total annual antibiotic production[6]. A large number of irregular uses of antibiotics in farming is one of the main sources of the spread of antibiotics, drug-resistant bacteria, and resistance genes to the environment, and excessive antibiotics will enter the environment directly or indirectly through the fecal and urinary pathways. Bacterial drug resistance has brought adverse effects on human society, such as increased biosecurity threats, intensified environmental pollution, and economic development constraints, which have aroused widespread concern around the world. Therefore, it is necessary to curb the development and spread of antibiotics and ARGs.

Due to the wide variety and complex structure of antibiotics, the existing conventional wastewater treatment process is difficult to treat them[7], which brings great challenges to the reduction and control of antibiotics. In response to this situation, researchers attempted to explore the development of efficient, economic, environmentally friendly new pollutant treatment technology. For the treatment of antibiotics and ARGs in water, the most common methods include biochar adsorption, advanced oxidation technology, and new environmental functional materials. At present, most of the reduction technologies of antibiotics and ARGs using biochar only have some drawbacks, such as secondary pollution and difficulty in recovery. And in practical applications, the adsorption effect of biochar will be greatly reduced due to the blockage of voids or the competition of adsorption sites[8]. For advanced oxidation technology, low recovery rate of carrier materials, low utilization rate of light source, and unexplained degradation mechanism are common in practical water treatment applications[9]. New environmental functional materials are a class of new materials with unique physical, chemical, or biological properties and good removal effect on pollutants[10–11]. The research, development, and application of new environmental functional materials have been the focus of attention. As an environmentally friendly material, biomass-based graphene functional material is expected to achieve large-scale low-cost production and has broad practical application prospects[12]. However, there are few studies on biomass-based graphene aerogels to degrade ARGs.

The invasive weed *Pedicularis kansuensis* Maxim. was first appeared in the Bayanbulak grassland around 2000, and now the harm area is increasing and beginning to spread to farmland[13]. At present, the invaded area of *Pedicularis kansuensis* Maxim. has reached 67,000 hectares, with an average coverage of 30% and a higher coverage of more than 80% (Fig. S1). At present, it is mainly removed by manual, mechanical, and other physical methods, but most of the *Pedicularis kansuensis* Maxim. is left by the side of the road, and there are few reports on how to effectively use *Pedicularis kansuensis* Maxim.. It is worth noting that *Pedicularis kansuensis* is a Tibetan medicine, and contains a variety of compounds such as iridoid glycosides, phenylethanolsides, alkaloids, flavonoids, lignans, etc. It has good biological activity in anti-inflammatory, antibacterial, anti-tumor, antiviral, and other aspects[14]. This provides a new way for us to prepare biomass-based aerogel for removing ARGs and antibiotic-resistant bacteria.

In this study, a biomass-based graphene aerogel (PKGA) was fabricated from *Pedicularis kansuensis* via a mild hydrothermal self-assembly method (95°C), which preserved the bioactive secondary metabolites

of the plant. PKGA was subsequently applied to remove ARGs from real swine wastewater. The specific objectives of this study were to: (i) evaluate the removal performance of PKGA toward ARGs in swine wastewater; (ii) characterize the changes in physicochemical properties and bacterial community structure of swine wastewater following PKGA application; and (iii) elucidate the relationships among ARG dynamics, physicochemical parameters, and microbial community shifts. The findings aim to provide a novel and sustainable strategy for ARG mitigation in livestock wastewater while offering an ecological pathway for the resource utilization of the invasive *Pedicularis kansuensis*.

2. Materials and methods

2.1 Materials and chemicals

Pedicularis kansuensis Maxim. (PK) was collected from Bayanbulak Alshat Grassland (42°54'N, 83°43'E); Graphene oxide (GO) was purchased from Suzhou Hengqiu Technology Co., LTD. L-Ascorbic acid (LAA) is purchased from Sinopsin Reagent Group. The experimental water was deionized water.

A pig farm located in a village of Fukang City, Xinjiang Province, China (44°9'N, 88°3'E), with an intensity of approximately fifty market hogs per year. Swine wastewater (25 L) was collected from the outlet of the sedimentation tank, stored in a sterilized plastic bucket, and transported to the laboratory by car refrigerator within 12h. The swine wastewater was filtered through 0.15-mm sterilized nylon gauze to remove large debris. The physicochemical properties of wastewater, including the pH, chemical oxygen demand (COD), total phosphorus (TP), and total nitrogen (TN), were analyzed following standard protocols. Detailed information on the wastewater parameters is presented in Table S1.

2.2 Preparation of PKGA

The preparation of PKGA follows the mature method of our team[15]. First, mix GO (3 mg/mL), PK, and LAA in a mass ratio of 4:2:1 and add the mixture to the reactor lining. After the solution was stirred evenly, the reactor liner was put into the reactor and sealed, and then put into a blast drying oven. After heating at 95℃ for 8 h, the *Pedicularis kansuensis* biomass-based graphene hydrogel (PKGH) was removed at room temperature and transferred to deionized water for soaking to remove impurities, and then the hydrogel was freeze-dried to obtain *Pedicularis kansuensis* biomass-based graphene aerogels (PKGA).

2.3 PKGA Characterization

The microscopic morphology of the samples was tested by SEM (S-4800, Hitachi, Japan); Energy Dispersive spectrometer (EDS, SU8010, Hitachi, Japan) was used to test material surface element composition; X-ray diffractometer (XRD, D8 Advance, Bruker, Germany) was for Material Phase analysis; Infrared spectroscopy (FTIR) was used for analysis of material functional group changes (VERTEX 70 RAMI, BRUKER, Germany); Thermo Gravimetric analyzer (TG) is used to test the thermal stability of materials (STA7300, Hitachi, Japan), the test process is carried out in a nitrogen atmosphere; X-ray photoelectron spectroscopy (XPS) is used for elemental state analysis on the surface of materials (K-

ALPHA, Thermo Field, USA); High Performance Surface Area and Aperture Analyzer is used to analyze the specific surface area and pore size of the material (BSD-660s A6B6, BSD Instrument, China). The authors would like to express their gratitude to Ceshigo Research Service (www.ceshigo.com) for providing the testing service.

2.4 Experimental setup and sample collection

Removal of ARGs from swine wastewater was based on the modified methods by Ngigi[16] and Wu[17]. The PKGA was conducted inside the triangular flask (with a working volume of 100 mL) to identify the accumulation on ARGs. Briefly, the PKGA was added at concentrations of 0 (CK), 5 (PKGA5), 20 (PKGA20), and 50 (PKGA50) mg/100mL. Each of the triangular flasks was placed in a shaker, which was set at 150 rpm and at a constant temperature of 25°C. Each treatment was repeated in 12 replicates. The schematic diagram of the PKGA preparation process and wastewater treatment is shown in Fig. 1.

On 1, 2, 3, and 4 weeks, three flasks were sampled randomly from each treatment as triplicates. A whole block of material was removed with sterile tweezers, then the 50 mL wastewater was used to analyze the pH, COD, TP, and TN. The 50mL residual wastewater was concentrated on 0.22-μm filters by a vacuum filtration apparatus, and the filters were stored in a sterile centrifuge tube at -20℃ for DNA extraction.

2.5 Real-time qPCR for ARGs

The relative quantification of ARGs (copies/16S rRNA gene) was evaluated by LightCycler480 II Real-Time PCR System (Roche, Rotkreuz, Switzerland). Specifically, the plasmid DNA with target genes was 10-fold serially diluted for making a standard curve by LightCycler480 II Real-Time PCR System (Roche, Rotkreuz, Switzerland). The qPCR mixtures consisted of 1 μl of template DNA, 0.2 μM concentration of each primer, 5 μl of SybrGreen qPCR Master Mix, and 3.6 μl of ddH_2O. The qPCR protocol was followed: 15 s at 95°C, 30 s at 60°C for 45 cycles, each point was run in triplicate. The specificity was verified by melting curves and gel electrophoresis. Targeting ARGs includes Sulfonamide Resistance genes [sul1, sul2], Macrolide Resistance genes [ermB, ermF], Tetracycline Resistance genes [tetA, tetC, tetW, and tetX], and Chloramphenicol resistance genes [cml(A1-01), cml(A1-02)]. In addition, the mobile genetic element [intl1] was also analyzed in this study, and the primer sequences were listed in Table S2[18]. The relative abundances of ARGs were calculated using the ΔCt method (Eqs. (1) and (2))[19].

$$\Delta Ct = Ct(ARG) - Ct(16S\ rRNA) \quad (1)$$

$$\text{Relative abundance of ARGs} = 2^{-\Delta Ct} \quad (2)$$

Where Ct was the amplification cycle, and Ct (ARG) and Ct (16S rRNA) referred to the threshold cycles of one ARG and the 16S rRNA gene, respectively.

2.6 Bacterial 16S rRNA gene sequencing and non-targeted metabolomic analysis

16S rRNA gene sequencing was conducted by Sangon Biotech. (Hangzhou, China). Briefly, for the analysis of the bacterial communities in the composting system, the V3-V4 region of the 16S rRNA gene was amplified by PCR using the primers 341F/805R. DNA samples were quantified using a Qubit 2.0 Fluorometer. The QIIME data analysis package was used for 16S rRNA data analysis. The operational taxonomic units (OTUs) were defined at the 97% similarity level. Sequences were rarefied before the calculation of alpha and beta diversity statistics. The sequencing data were deposited in the NCBI BioProject under the accession number PRJNA1180898.

PKGA was sent to Honsun Biological Technology CO., LTD (Shanghai, China) for non-targeted metabolomic analysis by using liquid chromatography-tandem mass spectrometry (LC-MS/MS). The precursor molecules in the positive and negative modes were then obtained to export the data.

2.7 Data and statistical analyses

The QIIME data analysis package was used for 16S rRNA data analysis. Statistical assessments were performed by SPSS 22.0 software. Bar charts were generated by Origin. Heatmaps were generated using R 3.5.2 with the pheatmap package. Shannon diversity, PCoA (Bray–Curtis distance–based), and distance-decay analyses were conducted using R with the vegan package. Non-metric Multidimensional Scaling (nMDS) plots were constructed by R. The functional prediction of the microbiome was analyzed by Tax4Fun (R package) with a SILVA database extension (SILVA 123).

3. Results

3.1 Characterization of PKGA and its intrinsic antibacterial properties

The microstructure and morphology of PKGA were characterized by SEM. As shown in Fig. 2a-b, PKGA is stacked by graphene sheets, showing a porous structure at the μm level. *Pedicularis kansuensis* tissue and graphene are closely combined through the aerogel, which helps to improve the overall mechanical strength of the composite. The stable network structure formed by graphene layers and plant tissue makes PKGA a lower-density material (Fig. 2c). These structures can make it have high porosity and specific surface area, which has an important influence on its adsorption of pollutants and microorganisms. As can be seen from Fig. 1d-f, PKGA is mainly composed of C and O elements, with a small amount of N elements. From the perspective of chemical composition, PKGA is an environmentally friendly carbon-based functional material.

The pore structure information of PKGA can be further studied by nitrogen adsorption and desorption curves. As can be seen from Fig. 3a, the adsorption and desorption isotherm of PKGA conforms to the Type II isotherm, indicating that PKGA is a macroporous structural material. According to BET and BJH model calculations, the specific surface area and pore volume of PKGA are 36.8954 m^2/g and 0.0961cm^3/g, respectively, which is caused by the existence of pore structures of different sizes in

PKGA, which has micropores with a pore size of 1.8518nm. Medium hole of 2.5513, 4.2386, and 6.4888 nm, large hole of 69.4945 nm.

Thermal analysis of PKGA can make a simple evaluation of its thermal stability, as shown in Fig. 3b. PKGA has partial weight loss due to water escape below 100°C, and large weight loss in the range of 200–400°C may be caused by the carbonization of *Pedicularis kansuensis* biomass, but overall, it can still maintain a high residual rate. This shows that PKGA has good thermal stability. As shown in Fig. 3c, the infrared spectrum shows that PKGA, as a carbon-based material, mainly has carbon-containing and oxygen-containing functional groups, among which the characteristic peaks at 3280.3 cm^{-1} are OH, and the characteristic peaks at 2921.6 and 2854.2 cm^{-1} are caused by CH_2. The characteristic peak at 1569.1 cm^{-1} is caused by C = C and C-C. Peaks near 1207.3 cm^{-1} and 1722.7cm^{-1} correspond to C-O-C and C = O, respectively. As shown in Fig. 3d, the characteristic diffraction peak appearing at 2θ = 22.1° corresponds to the (002) plane of GO, while the characteristic diffraction peak appearing at 2θ = 43.1° corresponds to the (100) plane of the graphite-carbon material. XPS further reveals the composition information of PKGA. It can be seen from Fig. 3e-f that PKGA is mainly composed of C and O. The fitting of the XPS fine spectrum shows that C1s has fitting peaks at C-C (284.8eV) and C-O (286.7eV).

Therefore, it can be seen from the above that PKGA is an environmentally friendly material with abundant pore structure and a large specific surface area, and is mainly composed of carbon and oxygen functional groups. The porous structure and rich functional group play an important role in the adsorption of pollutants in PKGA.

Notably, owing to the mild preparation temperature (95°C), the active chemical compositions of the Tibetan medicine *Pedicularis kansuensis* were well retained. Non-targeted metabolomic analysis by LC-MS/MS confirmed the presence of diverse plant secondary metabolites in PKGA, mainly including alkaloids, phenylethanoid glycosides (Fig. S2c), phenolic compounds (Fig. S2d), isoflavonoids (Fig. S2e), and flavonoids (Fig. S2f), which are known for their broad-spectrum biological activities. The retention of these active compounds endowed PKGA with inherent antibacterial properties. As shown in Fig. S2a-b, PKGA exhibited a significant inhibitory effect on the growth of *E. coli*. This dual functionality - combining the excellent physical adsorption capacity of graphene aerogel with the biological toxicity of plant metabolites toward bacteria - provides an innovative material basis for the elimination of antibiotic-resistant bacteria (ARB) and ARGs.

3.2 Changes in physicochemical properties of swine wastewater

The physicochemical parameters of swine wastewater during the PKGA treatment are summarized in Table 1. The pH of the wastewater remained relatively stable across all treatments, ranging from 7.43 to 7.90, indicating that PKGA application did not significantly alter the acid-base balance of the wastewater. However, COD decreased markedly with PKGA application. On day 7, COD in the PKGA50 treatment dropped to 130.00 mg/L compared to 338.60 mg/L in the CK group, representing a 61.6% reduction. By

day 56, COD values in PKGA20 and PKGA50 were further reduced to 112.00 and 108.60 mg/L, respectively, while CK still retained 206.67 mg/L.

Total phosphorus and total nitrogen also exhibited declining trends with the addition of PKGA. Total phosphorus in PKGA50 decreased from 5.44 mg/L (day 7) to 3.75 mg/L (day 56), and total nitrogen in PKGA50 declined from 17.67 mg/L (day 7) to 9.99 mg/L (day 56). Higher PKGA dosages generally led to greater reductions, indicating dose-dependent removal of nutrients.

Table 1
Chemical parameters of swine wastewater during adsorption

Time (Day)	Treatments	pH	COD (mg/L)	TP (mg/L)	TN (mg/L)
7	CK	7.90 ± 0.69	338.60 ± 22.40	6.01 ± 0.36	20.12 ± 1.51
	PKGA5	7.82 ± 0.66	200.00 ± 15.90	6.33 ± 0.50	20.78 ± 2.13
	PKGA20	7.80 ± 0.60	140.25 ± 12.60	6.36 ± 0.52	18.45 ± 1.36
	PKGA50	7.43 ± 0.56	130.00 ± 11.19	5.44 ± 0.48	17.67 ± 1.29
14	CK	7.70 ± 0.67	265.00 ± 18.53	5.96 ± 0.58	19.35 ± 1.96
	PKGA5	7.70 ± 0.65	190.67 ± 16.14	5.80 ± 0.63	19.16 ± 2.01
	PKGA20	7.69 ± 0.59	117.80 ± 19.19	5.01 ± 0.77	18.73 ± 1.55
	PKGA50	7.69 ± 0.58	102.77 ± 12.88	4.51 ± 0.47	16.44 ± 0.99
28	CK	7.76 ± 0.68	227.33 ± 15.64	5.84 ± 0.96	19.88 ± 2.33
	PKGA5	7.73 ± 0.65	187.80 ± 18.56	4.69 ± 1.16	19.56 ± 3.51
	PKGA20	7.60 ± 0.59	114.50 ± 18.90	4.92 ± 1.15	12.90 ± 3.18
	PKGA50	7.60 ± 0.57	108.20 ± 14.07	4.15 ± 0.99	10.68 ± 3.00
56	CK	7.58 ± 0.66	206.67 ± 17.08	5.44 ± 0.96	19.68 ± 2.13
	PKGA5	7.87 ± 0.66	165.00 ± 14.09	4.18 ± 1.21	18.84 ± 3.36
	PKGA20	7.56 ± 0.58	112.00 ± 11.88	4.18 ± 1.01	9.60 ± 2.98
	PKGA50	7.51 ± 0.57	108.60 ± 10.98	3.75 ± 0.94	9.99 ± 2.33

3.3 Removal of ARGs and intI1 by PKGA

The relative abundances of eleven ARGs and the MGE intI1 throughout the experiment are shown in Fig. 4a–k. All PKGA treatments significantly reduced ARG abundances relative to CK ($p < 0.05$), with removal efficiency positively correlated with dosage. Sulfonamide (sul1, sul2), tetracycline (tetA, tetC,

tetW, tetX), macrolide (ermB, ermF), and chloramphenicol resistance genes (cmlA1-01, cmlA1-02) were all suppressed effectively, while intI1 - a critical proxy for HGT potential—was simultaneously reduced.

The relative abundances of eleven targeted ARGs and the mobile genetic element intI1 were quantified throughout the experiment (Fig. 4a-k). All PKGA treatments significantly reduced the abundance of most ARGs compared to CK, and the removal efficiency was generally positively correlated with the PKGA dosage. Specifically, sulfonamide resistance genes (sul1, sul2), tetracycline resistance genes (tetA, tetC, tetW, tetX), macrolide resistance genes (ermB, ermF), and chloramphenicol resistance genes (cmlA1-01, cmlA1-02) were all effectively decreased by PKGA20 and PKGA50 treatments. The mobile genetic element intI1, which plays a key role in horizontal gene transfer, was also significantly reduced. The synchronous suppression of intI1 and ARGs strongly suggests that PKGA mitigates ARGs through a dual-layer regulatory mechanism: (i) direct removal of ARG-hosting bacteria via adsorption and antibacterial action, and (ii) blocking of horizontal gene transfer pathways through the suppression of intI1-mediated integron mobility[20]. This dual mechanism distinguishes PKGA from conventional adsorbents and represents one of its key advantages.

Correlation analysis (Fig. 4l) revealed that the abundance of ARGs was significantly positively correlated with COD, total phosphorus, and total nitrogen, suggesting that the reduction of organic matter and nutrients was closely associated with the decline of ARGs. This indicates that PKGA may simultaneously remove ARGs through both direct adsorption and indirect modulation of the wastewater chemical environment.

3.4 Effects of PKGA on the alpha diversity of bacterial communities

To further elucidate the ecological response of bacterial communities to PKGA application, four representative alpha diversity indices were calculated based on 16S rRNA gene sequencing data, including Chao and ACE indices reflecting community richness, as well as Shannon and Simpson indices reflecting community diversity and evenness (Fig. 5a–d).

As shown in Fig. 5a, the Chao index decreased significantly with increasing PKGA dosage. The CK group exhibited the highest Chao index (median = 530), suggesting that untreated swine wastewater harbored a relatively rich bacterial community. After the PKGA application, Chao values decreased to approximately 467, 455, and 443 in the PKGA5, PKGA20, and PKGA50 groups, respectively. Statistical analysis indicated that the CK group differed significantly from the PKGA5 group ($P < 0.05$) and exhibited highly significant differences from both the PKGA20 and PKGA50 groups ($P < 0.01$). A consistent trend was observed for the ACE index (Fig. 5b), with even more pronounced statistical significance. The ACE index decreased markedly from a median of approximately 545 (CK) to 384 (PKGA50). Significant differences ($P < 0.05$ to $P < 0.001$) were detected between the CK group and all PKGA-treated groups, as well as between PKGA50 and the lower-dose groups (PKGA5 and PKGA20, $P < 0.05$).

As illustrated in Fig. 5c, the Shannon index remained relatively stable among the CK, PKGA5, and PKGA20 groups, with median values ranging from approximately 2.13 to 2.22, indicating that low and moderate PKGA dosages exerted limited influence on the overall bacterial diversity. However, at the highest dosage (PKGA50), the Shannon index decreased markedly to approximately 1.61, and significant differences were observed between PKGA50 and both the CK and PKGA20 groups ($P < 0.05$). These results suggest that high-dose PKGA application significantly reduced the diversity of bacterial communities in swine wastewater. Consistently, the Simpson index (Fig. 5d) increased systematically with increasing PKGA dosage, rising from a median of approximately 0.24 in the CK group to 0.34, 0.44, and 0.48 in the PKGA5, PKGA20, and PKGA50 groups, respectively. Significant differences were detected between the CK group and the PKGA5 ($P < 0.05$), PKGA20 ($P < 0.01$), and PKGA50 ($P < 0.001$) groups, as well as between PKGA50 and PKGA5 ($P < 0.001$) or PKGA20 ($P < 0.05$), demonstrating a clear dose-dependent response.

Since the Simpson index reflects the degree of dominance within a community, the rising trend with PKGA dosage indicates that bacterial communities became progressively dominated by a few resilient taxa following PKGA treatment. This is in agreement with the decreasing trend of the Shannon index at high dosage. Taken together with the previously observed decrease in Chao and ACE indices, these results indicate that PKGA application reduced both bacterial richness and evenness, gradually reshaping the community from a relatively balanced structure toward a more dominance-driven configuration, with the most pronounced changes occurring under the PKGA50 treatment.

3.5 Regulation of bacterial community structure in swine wastewater by PKGA

The bacterial community composition at the phylum and genus levels was significantly altered by PKGA application (Fig. 6). As illustrated in Fig. 6a, the bacterial communities in swine wastewater were dominated by Proteobacteria, Bacteroidetes, Firmicutes, Spirochaetes, and unclassified_Bacteria, among which Proteobacteria consistently constituted the most abundant phylum. In the CK group, the relative abundance of Proteobacteria gradually increased from 60% at day 0 to 80% at day 56, indicating its progressive dominance over time. Following PKGA treatment, the relative abundance of Proteobacteria further increased in a dose-dependent manner, reaching 85%~95% in the PKGA20 and PKGA50 groups. These results suggest that PKGA selectively favored the survival of Proteobacteria-affiliated taxa, likely due to their stronger tolerance to nutrient limitation and antibacterial stress. In contrast, the relative abundance of Bacteroidetes decreased markedly after PKGA application, declining from 15%~20% in the CK group to approximately 5% in the PKGA20 and PKGA50 groups. A similar suppression trend was observed for Firmicutes, which was particularly pronounced under the PKGA50 treatment. The decline of Bacteroidetes and Firmicutes was closely associated with the overall reduction in ARG abundance (Fig. 4). Meanwhile, the relative abundances of Spirochaetes and unclassified_Bacteria slightly increased in the PKGA-treated groups, indicating that suppression of originally dominant taxa released ecological niches for low-abundance microorganisms.

Genus-level analysis (Fig. 6b) further revealed the selective regulation of bacterial communities by PKGA. *Advenella*, *Alcaligenes*, and *Arcobacter* were the dominant genera in the CK group, jointly accounting for 30%~40% of the community in the early stage. However, following PKGA treatment, their relative abundances rapidly declined, particularly in the PKGA20 and PKGA50 groups. Concurrently, *Acinetobacter* was significantly enriched in PKGA-treated systems, reaching over 70% relative abundance in the PKGA20 and PKGA50 groups at days 14–28. *Acinetobacter*, an aerobic to facultative anaerobic genus with strong tolerance to oligotrophic and antibacterial stress, appeared to benefit from the selective microenvironment established by PKGA. And environmentally resilient and non-typical ARG-hosting genera such as *Sphingomonas* and *Achromobacter* exhibited slight enrichment.

Overall, the genus-level community response to PKGA exhibited a clear bidirectional pattern: suppression of ARG-hosting genera (e.g., *Arcobacter*, *Advenella*, *Alcaligenes*) coupled with enrichment of tolerant non-ARG-hosting genera (e.g., *Acinetobacter*, *Sphingomonas*). This dual regulatory pattern provides a key microbiological basis for the effective ARG mitigation achieved by PKGA.

3.6 Correlation analysis among genera, ARGs, MGEs, and environmental factors

To elucidate the intrinsic linkage between PKGA-induced community restructuring and ARG attenuation, a Spearman correlation analysis was conducted among 13 genera (microorganisms at the genus level with relative abundance ranking in the top 13), 10 ARGs, the mobile genetic element intI1, and four key environmental factors (pH, COD, TN, and TP) (Fig. 7a).

As shown in Fig. 7a, the heatmap exhibited a distinct bi-clustering pattern: the left cluster of 8 genera (*Acinetobacter*, *Advenella*, *Alcaligenes*, *Bacteroides*, *Arcobacter*, *Sphaerochaeta*, and *Macellibacteroides*) was generally positively correlated with ARGs and nutrient factors (red region), whereas the right cluster of 6 genera (*Sedimentibacter*, *Pseudomonas*, *Cloacibacterium*, *Microvirgula*, *Sphingomonas*, and *Achromobacter*) was significantly negatively correlated with ARGs, intI1, and nutrient factors (blue region). Specifically, *Advenella* and *Pseudomonas* showed significant positive correlations with sul1, and *Bacteroides* exhibited significant positive correlations with ermB and tetX ($P < 0.01$). The strong positive correlations between *Arcobacter* and tetX/COD ($P < 0.01$) further confirm its role as an important carrier of pathogenic resistant bacteria in swine wastewater. The three anaerobic/microaerobic genera *Sphaerochaeta*, *Macellibacteroides*, and *Sedimentibacter* exhibited moderate positive correlations with sul1, ermB, tetX, and ermF, constituting the anaerobic ARG-hosting subset in swine wastewater.

All 6 right-cluster genera exhibited significant to highly significant negative correlations with sul1, sul2, tetA, tetC, cmlA-01, cmlA-02, intI1, TN, TP, and COD ($P < 0.05$ to $P < 0.001$). Notably, TN and TP showed negative correlations with most right clusters of genera (*Sedimentibacter*, *Pseudomonas*, *Cloacibacterium*, *Microvirgula*, *Sphingomonas*, and *Achromobacter*). Similarly, tetA, cmlA-02, and intI1 showed negative correlations with *Cloacibacterium*, *Microvirgula*, and *Sphingomonas*. The highly significant negative correlations of *Sphingomonas* and *Microvirgula* with intI1, TN, and TP indicate that

these genera are not major hosts of ARGs and that their enrichment paralleled the synchronous decline of nutrient concentrations and ARG abundances. Notably, *Pseudomonas* exhibited a positive correlation with sul1 but a significant negative correlation with tetC, revealing a differential carrier pattern of ARGs within the *Pseudomonas* community under PKGA treatment.

3.7 KEGG functional pathway prediction based on Tax4Fun

To further elucidate the regulatory mechanism of PKGA at the functional level, Tax4Fun-based functional prediction was conducted on the 16S rRNA gene data, yielding the relative abundance variations of 35 KEGG Level-2 functional pathways (Fig. 7b).

As shown in Fig. 7b, the functional potential of the bacterial community was substantially reshaped after PKGA treatment, displaying a bidirectional pattern characterized by “downregulation of metabolic and disease-related functions coupled with upregulation of xenobiotics biodegradation functions”, with the magnitude of restructuring positively dependent on PKGA dosage. In general, metabolism-related functions were globally downregulated. Core metabolic pathways, including Amino Acid Metabolism, Carbohydrate Metabolism, Energy Metabolism, Lipid Metabolism, Nucleotide Metabolism, and Metabolism of Cofactors and Vitamins, were significantly downregulated in the PKGA20 and PKGA50 groups. The CK group exhibited predominantly red signals at the early stage, reflecting the high metabolic activity driven by nutrient enrichment in raw swine wastewater. In contrast, the PKGA50 group at the later stage (PKGA50-28, PKGA50-56) displayed predominantly blue signals, indicating that PKGA-induced oligotrophication (through removal of organic matter and nutrients) suppressed the metabolic activity of copiotrophic taxa. This result is mutually corroborated by the decline of Bacteroidetes and Firmicutes at the phylum level (Fig. 6a) and the positive correlations of TN, TP, and COD with ARGs in the correlation analysis (Fig. 4l). Furthermore, human disease–related functions were significantly downregulated in the PKGA-treated groups. Pathways including Infectious Diseases, Cancers, Cardiovascular Diseases, Neurodegenerative Diseases, Metabolic Diseases, and Immune System Diseases all displayed pronounced blue signals in the PKGA20 and PKGA50 groups. Instead, Xenobiotics Biodegradation and Metabolism functions were upregulated in PKGA-treated groups. This pathway exhibited pronounced red signals in the PKGA20 and PKGA50 groups.

In brief, PKGA treatment drove a functional transition of the swine wastewater microbial community from a “nutrient-rich, pathogenic, ARG-hosting” functional configuration to an “oligotrophic, biosafe, degradation-capable” functional configuration, providing critical functional-level support for the efficient mitigation of ARGs.

4. Discussion

4.1 Multifunctional structure of PKGA facilitates ARG removal

The successful preparation of PKGA via mild hydrothermal reduction (95°C) preserved the bioactive components of "*Pedicularis kansuensis*" while constructing a three-dimensional interconnected porous graphene network. This hierarchical porous structure provides a large specific surface area and abundant adsorption sites for the capture of pollutants and microorganisms[21]. The presence of oxygen-containing functional groups (–OH, –COOH, C = O) confirmed by FT-IR and XPS analyses enhances the surface hydrophilicity and provides additional binding sites for interactions with extracellular DNA and bacterial cells through hydrogen bonding, electrostatic interactions, and π-π stacking[22–23].

Compared with conventional biochar adsorbents, the three-dimensional graphene aerogel structure offers superior mass transfer efficiency and easy recovery, addressing the secondary pollution issues of powdered adsorbents. Furthermore, the incorporation of *Pedicularis kansuensis*-derived bioactive metabolites endows PKGA with intrinsic antibacterial properties, distinguishing it from conventional graphene-based materials that primarily rely on physical adsorption.

4.2 Reshaping of bacterial community structure and metabolic functions

PKGA application effectively reduced the overall bacterial richness in swine wastewater, particularly under high-dose conditions. This decrease in richness is likely attributable to (i) physical entrapment of bacterial cells within the three-dimensional porous network of PKGA, (ii) nutrient depletion (e.g., reductions in COD, TN, and TP, as shown in Table 1) that suppresses the growth of nutrient-demanding taxa, and (iii) selective inhibition by retained bioactive metabolites originating from *Pedicularis kansuensis*, including flavonoids, alkaloids, iridoid glycosides, and phenylethanoid glycosides, as confirmed by the metabolomic analysis (Fig. S2).

In addition, the PKGA application significantly altered the bacterial community composition by reducing the relative abundance of Firmicutes and Bacteroidetes, which are recognized as major reservoirs of ARGs[24–25]. Notably, *Arcobacter*, a well-recognized opportunistic pathogen and reported host of multiple ARGs (e.g., tetA, tetX, and sul1)[26–27], was substantially suppressed by PKGA, suggesting a targeted attenuation effect on potentially pathogenic ARG-hosting taxa. *Bacteroides* exhibited significant positive correlations with ermB and tetX ($P < 0.01$), in agreement with previous reports identifying *Bacteroides* as a major host of ermB and tetX[28]. TN, TP, and COD were positively correlated with most ARGs, consistent with previous reports that elevated nutrient levels facilitate the proliferation of ARG-hosting bacteria and HGT processes[29]. The $P < 0.001$ level negative correlations between TN/TP and the right 6 genera (*Sedimentibacter*, *Pseudomonas*, *Cloacibacterium*, *Microvirgula*, *Sphingomonas*, and *Achromobacter*) indicate that PKGA-mediated nutrient depletion directly drove the enrichment of the non-resistant cluster, thereby establishing a "nutrient depletion → community restructuring → HGT blockade → ARG attenuation" cascading regulatory pathway. Notably, *Pseudomonas* exhibited a positive correlation with sul1 (non-significant) but a significant negative correlation with tetC ($p < 0.05$). This contrasting pattern reflects the differential genetic carriers and transmission pathways of these two ARGs. Specifically, sul1 is typically tightly coupled with Class 1 integrons (intI1) and stably integrated into the chromosome or

plasmids of *Pseudomonas*[20], and may persist as a “baseline ARG” even during strain-level succession. In contrast, tetC is mainly carried by Enterobacteriaceae and Bacteroidetes[30] and is rarely retained in *Pseudomonas*. Therefore, the increase in total *Pseudomonas* abundance produced a “baseline retention effect” for sul1 but a “community replacement effect” for tetC. This finding highlights that the risk assessment of ARGs in multifunctional taxa should integrate genetic carriers, host distribution, and transmission pathways, rather than relying solely on genus-level abundance variations[31].

Combined with the significant decline or functional succession of pathogenic genera (*Arcobacter*, *Alcaligenes*, *Acinetobacter*) under PKGA treatment (Fig. 6b and Fig. 7), it can be inferred that PKGA indirectly attenuated human disease–related functional potentials by suppressing pathogenic taxa, thereby substantially enhancing the biosafety of the wastewater. Genetic Information Processing functions were downregulated in the PKGA50 group. On the other hand, core pathways, including Replication and Repair, Translation, and Transcription, were all downregulated in the PKGA50 group, indicating that high-dose PKGA, through the synergistic action of physical adsorption, nutrient limitation, and natural antibacterial metabolites, suppressed core microbial proliferation and gene expression functions, thereby further reducing the potential risk of ARG replication and dissemination. Instead, Xenobiotics Biodegradation and Metabolism functions were upregulated in PKGA-treated groups. This pathway exhibited pronounced red signals in the PKGA20 and PKGA50 groups. The Xenobiotics Biodegradation and Metabolism pathway encompasses microbial degradation of aromatic hydrocarbons, antibiotics, and other recalcitrant organic compounds[32], and the PKGA-enriched genera Sphingomonas and Achromobacter are recognized as core taxa responsible for such degradation functions[33]. This indicates that PKGA treatment not only attenuates antibiotics and ARGs through physical adsorption but also enables synergistic biodegradation of antibiotic residues through the enrichment and succession of degradation-capable microorganisms, thereby enhancing the robustness and completeness of ARG mitigation.

4.3 Mechanisms of ARG reduction by PKGA

The significant reduction of ARGs by PKGA can be attributed to multiple synergistic mechanisms. First, the porous graphene scaffold directly adsorbs extracellular ARGs and ARG-carrying bacteria from the wastewater through physicochemical interactions[34]. The strong positive correlation between ARG abundance and COD/TN/TP confirms that the reduction of organic matter and nutrients via adsorption indirectly limits the proliferation of ARG-hosting bacteria, as nutrient limitation suppresses bacterial growth and horizontal gene transfer[35].

Second, the bioactive compounds released from *Pedicularis kansuensis*, including iridoid glycosides, phenylethanoid glycosides, and flavonoids, possess broad-spectrum antibacterial activity[36–37]. The metabolomic analysis confirmed the abundance of these compounds in PKGA, and the antibacterial assay against *E. coli* validated their bactericidal effect.

Third, the reduction of the mobile genetic element intI1 is particularly important, as class 1 integrons play a critical role in the horizontal transfer and dissemination of ARGs[20]. The decrease in intI1 abundance suggests that PKGA effectively curbs the horizontal gene transfer potential within the bacterial community, thereby limiting the spread of antibiotic resistance.

5. Conclusions

In this study, a novel biomass-based graphene aerogel (PKGA) was successfully fabricated from the invasive Tibetan medicinal plant *Pedicularis kansuensis* Maxim. via a mild hydrothermal self-assembly approach, and its performance for ARG removal in swine wastewater was systematically evaluated. The major conclusions are summarized as follows:

(1) Material characteristics and dual functionality. PKGA exhibited a hierarchical macro-meso-microporous structure (SBET = 36.90 m^2/g; pore volume = 0.0961 cm^3/g), abundant oxygen-containing functional groups, and significant carbon defects (ID/IG > 1). The mild preparation temperature (95°C) successfully preserved the bioactive secondary metabolites of *Pedicularis kansuensis*, conferring intrinsic antibacterial activity on PKGA. This dual functionality—graphene-based physical adsorption combined with plant-derived biological inhibition—constitutes the material foundation for synergistic ARG removal.

(2) Effective improvement of wastewater quality. PKGA application led to dose-dependent reductions in COD, total nitrogen, and total phosphorus. At a dosage of 50 mg/100 mL, COD decreased by 61.6% within 7 days and was further reduced to 108.60 mg/L by day 56, demonstrating the strong removal capacity of PKGA for both organic pollutants and nutrients.

(3) Significant suppression of ARGs and intI1. PKGA significantly reduced the relative abundances of eleven targeted ARGs and the mobile genetic element intI1, with the highest dosage (PKGA50) achieving the most pronounced suppression. The simultaneous suppression of intI1 indicates that PKGA inhibits horizontal gene transfer (HGT) at the genetic-element level, providing dual-layer regulation of ARGs (host inhibition + HGT blocking).

(4) Reshaping of bacterial community structure. PKGA application markedly altered the bacterial community in swine wastewater by suppressing typical ARG-hosting taxa such as Bacteroides, Sedimentibacter, and Macellibacteroides, while enriching multifunctional genera, particularly *Pseudomonas*. Strain-level analysis suggested that PKGA selectively favored non-pathogenic, degradation-capable *Pseudomonas* strains, driving a functional succession from ARG-carrying to non-resistant types within the *Pseudomonas* community.

(5) Differential carrier patterns of ARGs in Pseudomonas. *Pseudomonas* exhibited a positive correlation with sul1 but a significant negative correlation with tetC, revealing differential ARG carrier characteristics governed by gene-specific genetic backbones (chromosomal integron-associated sul1 vs. conjugative-plasmid-associated tetC). This finding highlights that the risk assessment of ARGs in multifunctional

taxa should integrate genetic carriers, host distribution, and transmission pathways, rather than relying solely on genus-level abundance.

(6) Ecological and applied significance. This study not only proposes an innovative dual-mechanism material for ARG control in livestock wastewater, but also provides a sustainable utilization pathway for the invasive, harmful plant *Pedicularis kansuensis*, achieving the synergistic objective of “ecological remediation by ecological harm.” The findings may offer theoretical and practical references for the development of multifunctional biomass-based environmental materials and the green management of antibiotic resistance pollution.

Future studies should focus on: (i) elucidating the molecular mechanisms by which specific *Pedicularis kansuensis* metabolites disrupt resistant bacteria and ARGs; (ii) evaluating the performance of PKGA in continuous flow and pilot-scale systems; and (iii) exploring the regeneration and reusability of PKGA for long-term engineering applications.

Declarations

Competing interests

The authors declare no competing interests. The authors declare that they have no known competing financial interests or personal relationships that could have appeared to influence the work reported in this paper.

Author Contribution

L.S. conceived the idea for the review paper and wrote the first draft. W.F., C.M., W.-Y.X., D.J., and A.M. provided the content for multiple sections and edited multiple versions of the paper. W.-S.S. and J.-H.T. reviewed and edited the manuscript.

Acknowledgements

This work was supported by the National Postdoctoral Science Foundation of China (2021M693897), the National Natural Science Foundation of China (32460684), the Natural Science Foundation of Xinjiang Uygur Autonomous Region (2023D01B37), the Xinjiang Uygur Autonomous Region “Three Rural” Backbone Training Project (2023SNGGGCC002), and the Xinjiang Key Laboratory for Ecological Adaptation and Evolution of Extreme Environment Organisms (XKLEAEEEO-09).

References

1. Xu, L. et al. Occurrence, fate, and risk assessment of typical tetracycline antibiotics in the aquatic environment: a review. *Sci. Total Environ.* 753, 141975 (2021).
2. Muurinen, J. et al. Influence of manure application on the environmental resistome under finnish agricultural practice with restricted antibiotic use. *Environ. Sci. Technol*. 51, 5989–5999 (2017).
3. Miranda, C. D., Kehrenberg, C., Ulep, C., Schwarz, S. & Roberts, M. C. Diversity of tetracycline resistance genes in bacteria from chilean salmon farms. Antimicrob. Agents. *Chemother.* 47, 883–888 (2003).
4. Theriot, C. M. et al. Antibiotic-induced shifts in the mouse gut microbiome and metabolome increase susceptibility to clostridium difficile infection. *Nat. Commun.* 5, 3114 (2014).
5. Zhang, G., Zhang, D. & Li, W. Antagonistic effects of microplastic biofilms on antibiotic resistance gene horizontal transfer in water environments. *Aquat. Toxicol.* 293, 107766 (2026).
6. Zhang, Q., Ying, G., Pan, C., Liu, Y. & Zhao, J. Comprehensive evaluation of antibiotics emission and fate in the river basins of china: source analysis, multimedia modeling, and linkage to bacterial resistance. *Environ. Sci. Technol.* 49, 6772–6782 (2015).
7. Deng, Y., Mao, Y., Li, B., Yang, C. & Zhang, T. Aerobic degradation of sulfadiazine byarthrobacter spp.: Kinetics, pathways, and genomic characterization. *Environ. Sci. Technol.* 50, 9566–9575 (2016).
8. Yao, Y. et al. Removal of phosphate from aqueous solution by biochar derived from anaerobically digested sugar beet tailings. *J. Hazard. Mater.* 190, 501–507 (2011).
9. Li, Y. et al. Oxidative degradation of sulfamethoxazole antibiotic catalyzed by porous magnetic manganese ferrite nanoparticles: mechanism and by-products identification. *J. Mater. Sci.* 55, 13767–13784 (2020).
10. Zheng, M., Shao, Y., Ma, F., Li, W. & Guo, M. Adsorption of antibiotics in medical wastewater by mof-based hydrogel composites: a comprehensive review. *J. Water Process. Eng.* 76, 108268 (2025).
11. Godiya, C. B. & Leiviskä, T. Wood-derived adsorbents for the removal of pharmaceutical contamination from wastewater: a review. *Environ. Chem. Lett.* 24, 347–377 (2026).
12. Tripathi, V. K. et al. Biomass-based graphene aerogel for the removal of emerging pollutants from wastewater. *React. Chem. Eng.* 9, 753–776 (2024).
13. Zhai, G. et al. Adsorption of sulfadiazine from water by pedicularis kansuensis derived biochar: preparation and properties studies. *J. Ind. Eng. Chem*. 143, 581–591 (2025).
14. Li, M., He, X., Tao, R. & Cao, X. Phytochemistry and pharmacology of the genuspedicularis used in traditional chinese medicine. *The American Journal of Chinese Medicine* 42, 1071–1098 (2014).
15. Liu, S. et al. Hydrophobic pedicularis kansuensis/graphene aerogel with solar thermal effect enables efficient removal of sulfadiazine and oil from water. *J. Environ. Manage.* 377, 124618 (2025).
16. Ngigi, A. N., Ok, Y. S. & Thiele-Bruhn, S. Biochar-mediated sorption of antibiotics in pig manure. *J. Hazard. Mater*. 364, 663–670 (2019).
17. Wu, J. et al. Fate and removal of antibiotic resistance genes in heavy metals and dye co-contaminated wastewater treatment system amended with β-cyclodextrin functionalized biochar.

Sci. Total Environ. 723, 137991 (2020).

18. Wang, S. et al. Selectively enrichment of antibiotics and args by microplastics in river, estuary and marine waters. *Sci. Total Environ*. 708, 134594 (2020).
19. Zhang, S. et al. Effect of antibiotics, antibiotic-resistant bacteria, and extracellular antibiotic resistance genes on the fate of args in marine sediments. *Sci. Total Environ.* 891, 164305 (2023).
20. Gillings, M. R. et al. Using the class 1 integron-integrase gene as a proxy for anthropogenic pollution. *The Isme Journal* 9, 1269–1279 (2015).
21. Chen, J. et al. Bacterial community shift and antibiotics resistant genes analysis in response to biodegradation of oxytetracycline in dual graphene modified bioelectrode microbial fuel cell. *Bioresour. Technol.* 276, 236–243 (2019).
22. Yu, F., Sun, S., Han, S., Zheng, J. & Ma, J. Adsorption removal of ciprofloxacin by multi-walled carbon nanotubes with different oxygen contents from aqueous solutions. *Chem. Eng. J.* 285, 588–595 (2016).
23. Ren, W. et al. Origins of electron-transfer regime in persulfate-based nonradical oxidation processes. *Environ. Sci. Technol.* 56, 78–97 (2022).
24. Forsberg, K. J. et al. Bacterial phylogeny structures soil resistomes across habitats. *Nature* 509, 612–616 (2014).
25. Hu, Y. et al. The bacterial mobile resistome transfer network connecting the animal and human microbiomes. *Appl. Environ. Microbiol.* 82, 6672–6681 (2016).
26. Dekić Rozman, S., Puljko, A., Karkman, A., Virta, M. & Udiković-Kolić, N. Bacterial hosts of clinically significant beta-lactamase genes in croatian wastewaters. *Fems Microbiol. Ecol.* 100, fiae81 (2024).
27. Xiao, C. et al. Metagenomic profiling of antibiotic resistance genes and their associations with the bacterial community along the kanda river, an urban river in japan. *J. Biosci. Bioeng.* 139, 147–155 (2025).
28. Salyers, A., Gupta, A. & Wang, Y. Human intestinal bacteria as reservoirs for antibiotic resistance genes. *Trends Microbiol.* 12, 412–416 (2004).
29. Chen, W., Li, S., Chen, C. & Yan, L. Self-assembly and embedding of nanoparticles by in situ reduced graphene for preparation of a 3d graphene/nanoparticle aerogel. *Adv. Mater.* 23, 5679–5683 (2011).
30. Roberts, M. C. Update on acquired tetracycline resistance genes. *Fems Microbiol. Lett.* 245, 195–203 (2005).
31. Partridge, S. R., Kwong, S. M., Firth, N. & Jensen, S. O. Mobile genetic elements associated with antimicrobial resistance. *Clin. Microbiol. Rev.* 31, e17-e88 (2018).
32. Kanehisa, M., Sato, Y., Furumichi, M., Morishima, K. & Tanabe, M. New approach for understanding genome variations in kegg. *Nucleic. Acids. Res.* 47, D590-D595 (2019).
33. Stolz, A. Molecular characteristics of xenobiotic-degrading sphingomonads. *Appl. Microbiol. Biotechnol.* 81, 793–811 (2009).

34. Yu, F., Bai, X., Liang, M. & Ma, J. Recent progress on metal-organic framework-derived porous carbon and its composite for pollutant adsorption from liquid phase. *Chem. Eng. J.* 405, 126960 (2021).
35. Zhang, Y. et al. Temporal succession of soil antibiotic resistance genes following application of swine, cattle and poultry manures spiked with or without antibiotics. *Environ. Pollut.* 231, 1621–1632 (2017).
36. Khodaie, L., Bamdad, S., Delazar, A. & Nazemiyeh, H. Antioxidant, total phenol and flavonoid contents of two pedicularis l. Species from eastern azerbaijan, iran. *Bioimpacts: Bi* 2, 43–57 (2012).
37. Ma, S. et al. Chemical constituents of pedicularis kansuensis. *Chem. Nat. Compd.* 53, 586–588 (2017).

Figures

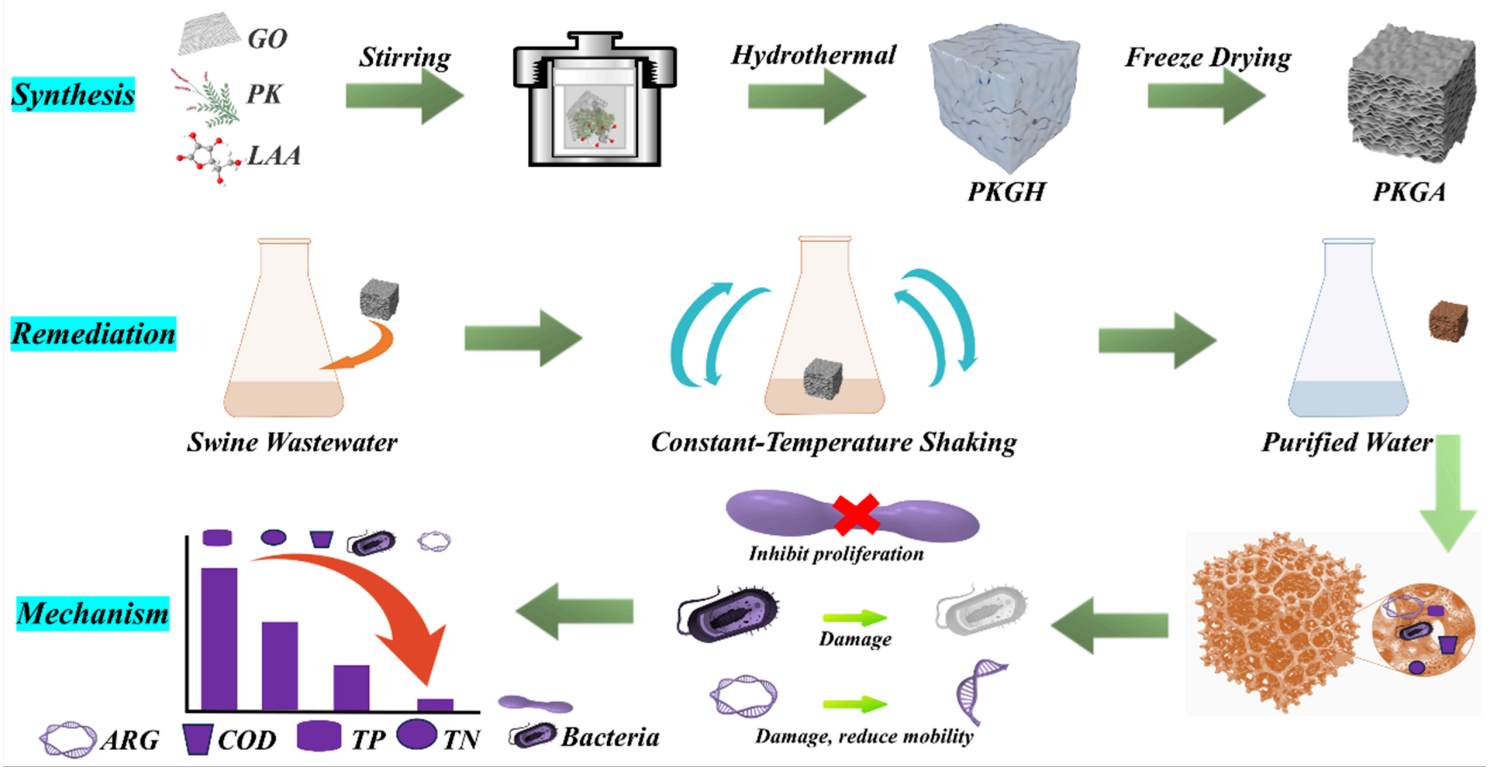


Figure 1

Schematic Diagram of the PKGA Preparation Process, Wastewater Treatment, and Mechanism

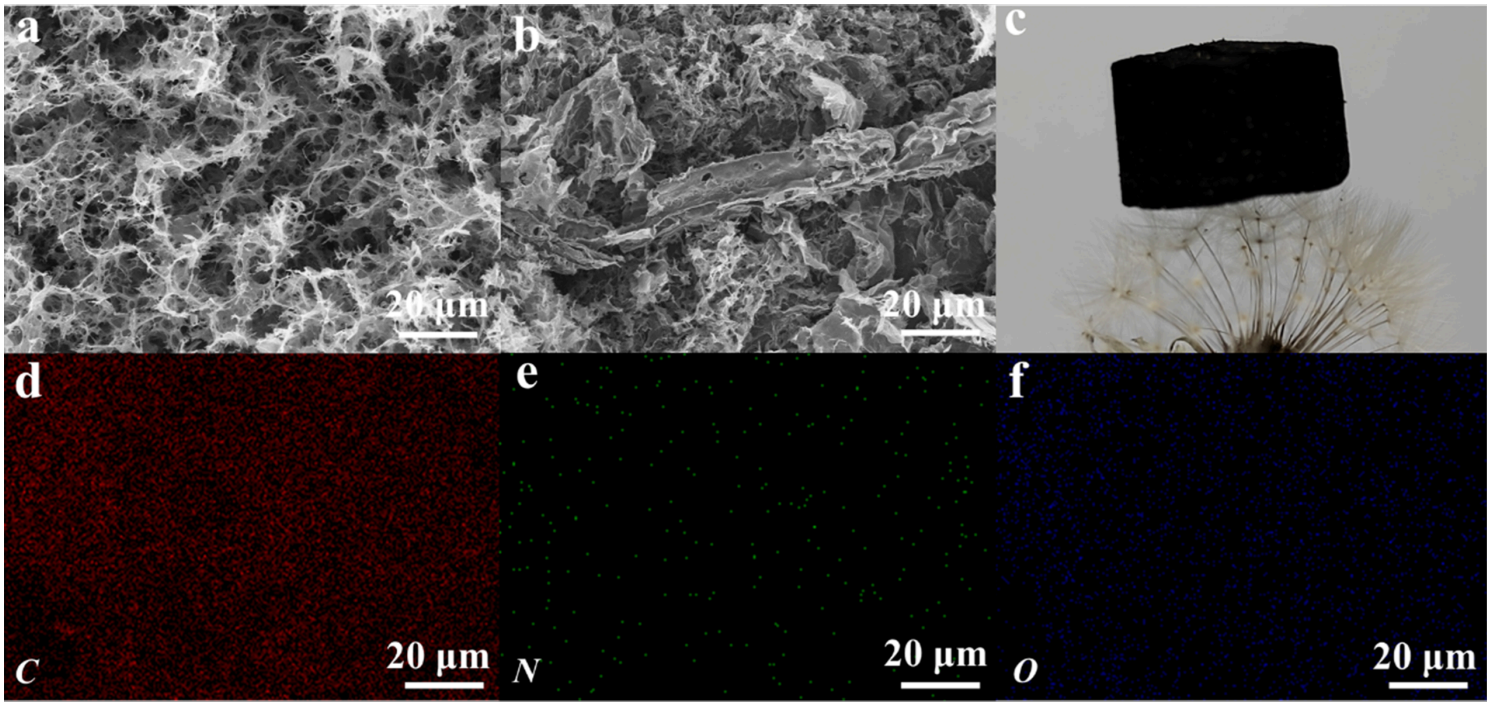


Figure 2

SEM (a-b), optical photograph (c), and EDS (d-f) of PKGA

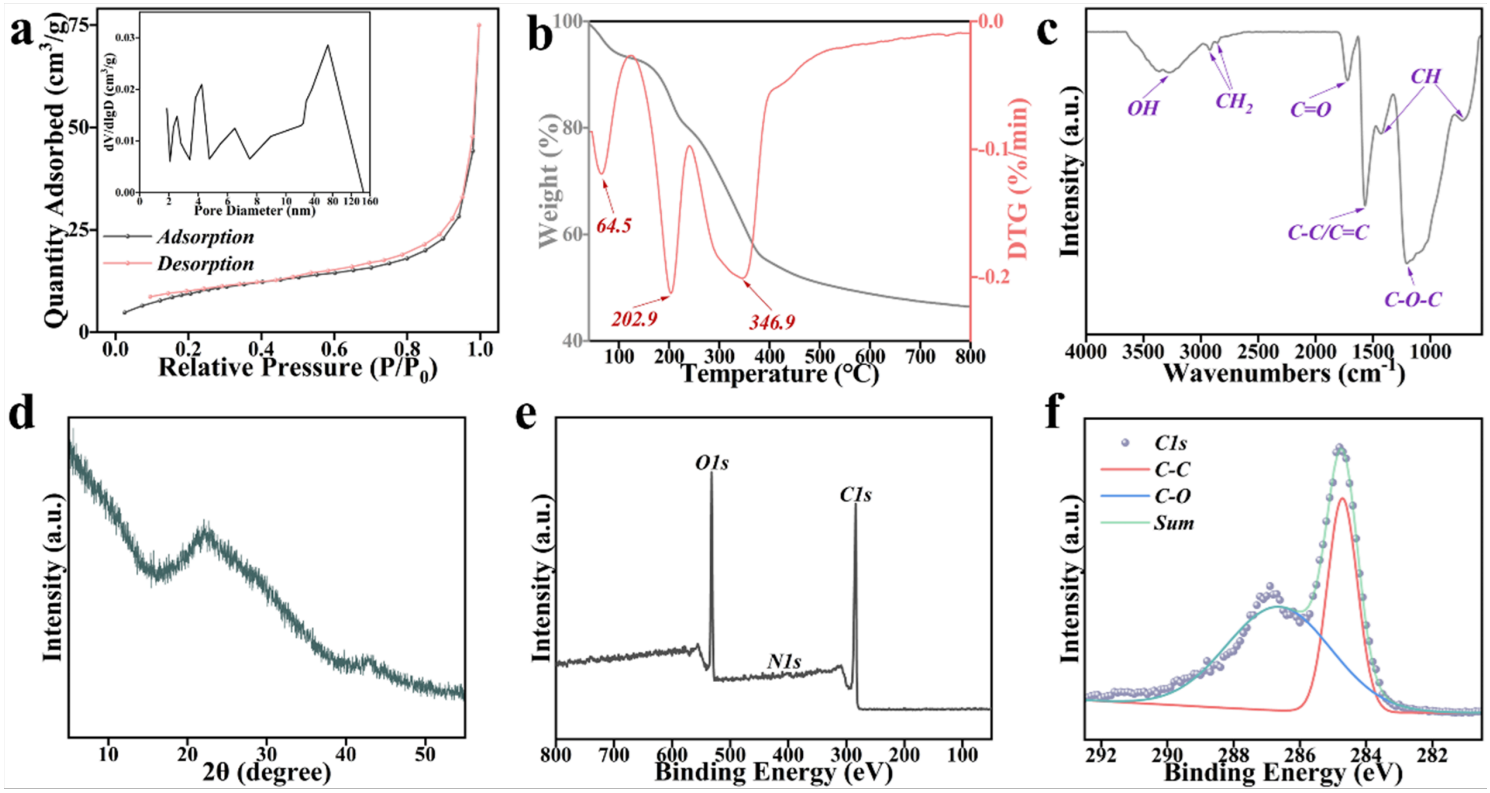


Figure 3

N_2 adsorption/desorption isotherm and pore size distribution (a), TG (b), FTIR-ATR (c), XRD pattern (d), and XPS Full Spectrum (e-f) of PKGA

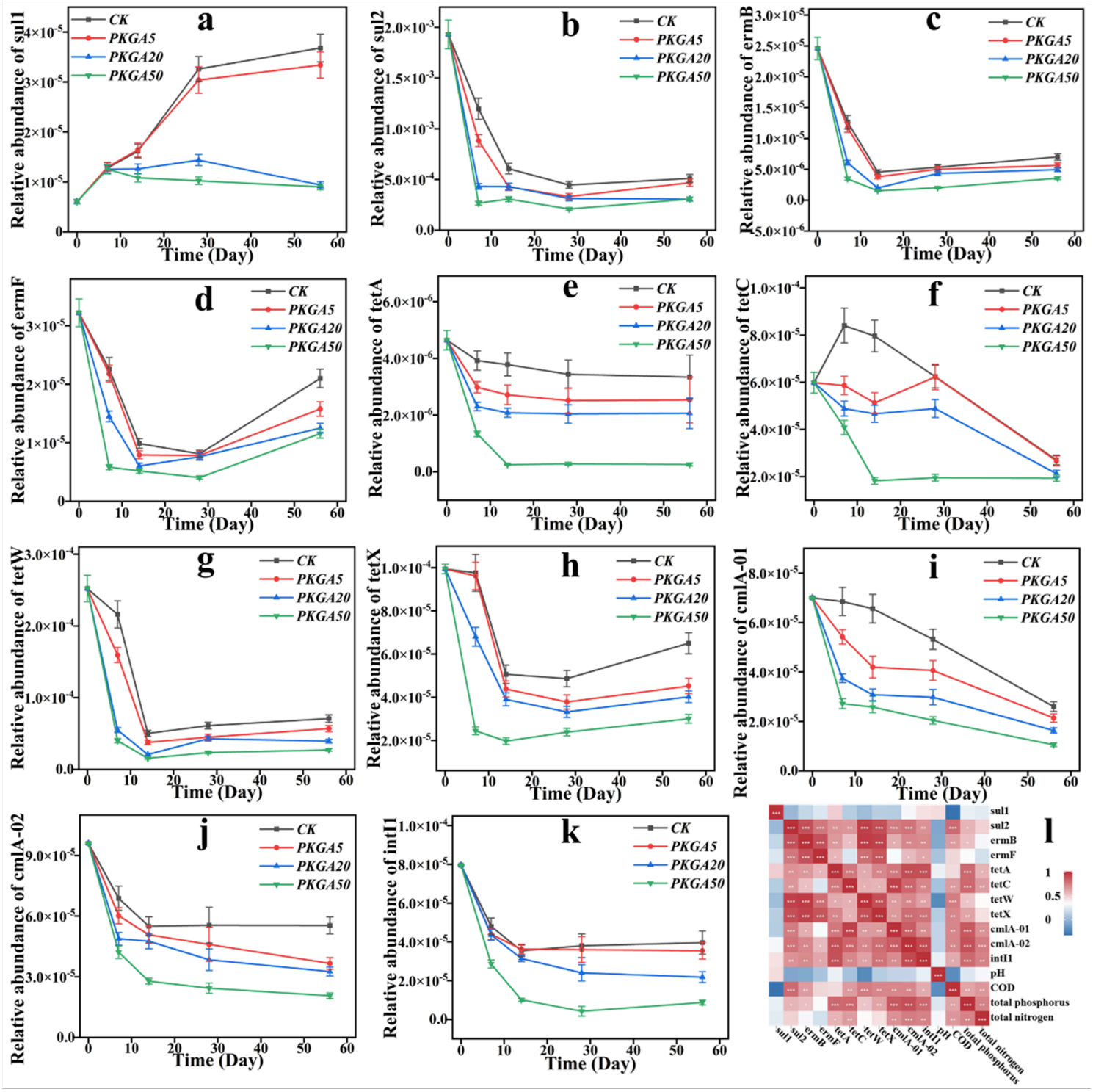


Figure 4

The adsorption curve of PKGA on ten antibiotic resistance genes (a-j), one mobile genetic element (intI1), and the correlation between resistance genes and physicochemical properties of water bodies (l)

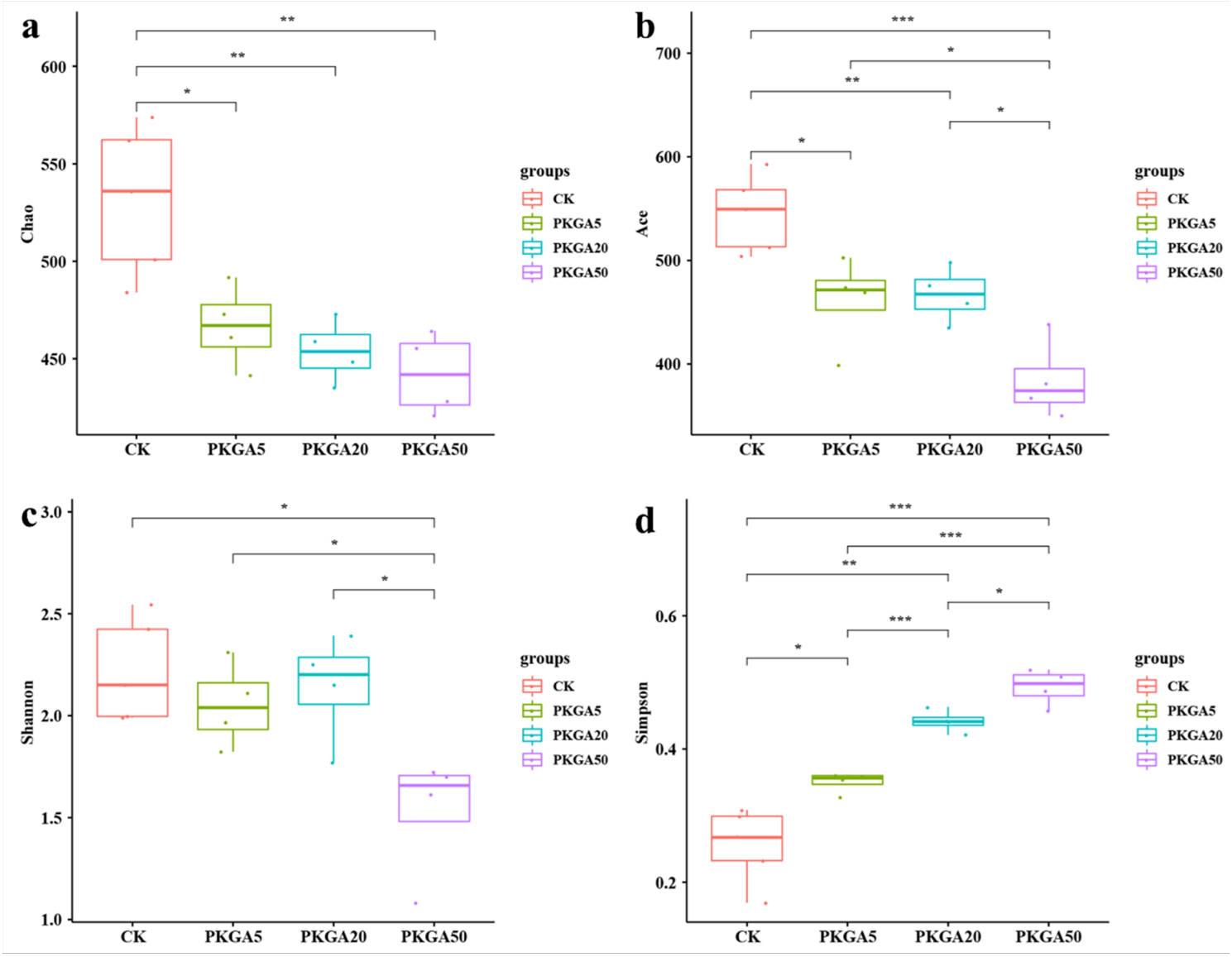


Figure 5

Effects of PKGA on the alpha diversity of bacterial communities (a: Chao index; b: Ace index; c: Shannon index; d: Simpson index)

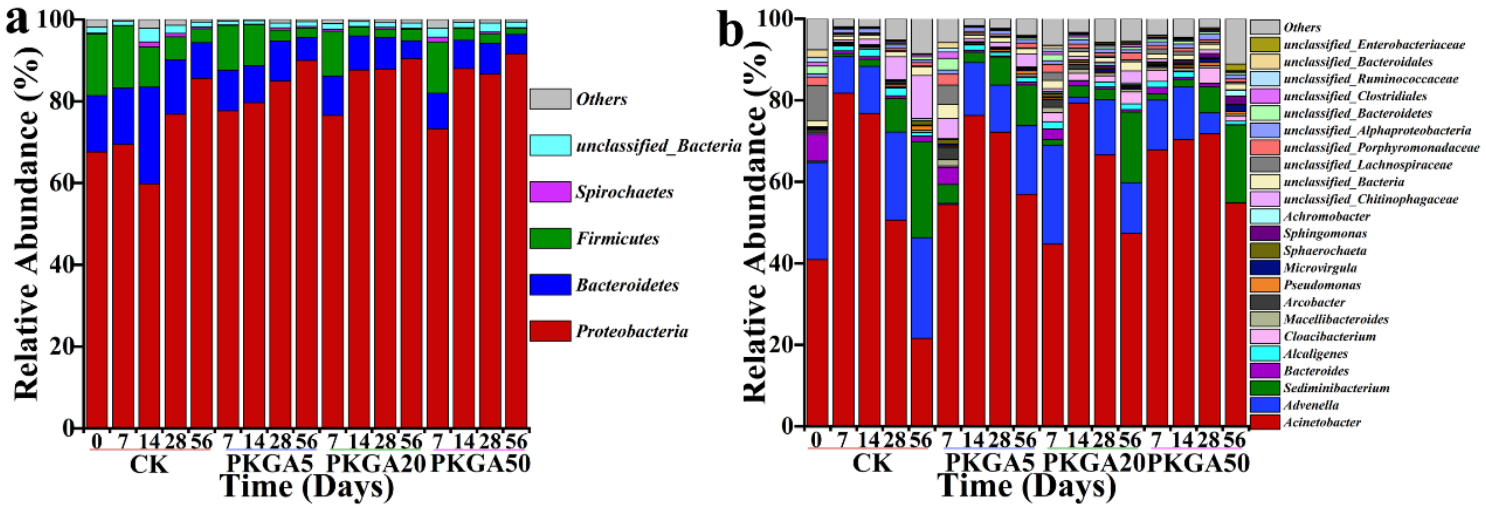


Figure 6

Effects of PKGA on the bacterial community structure (a: Phylum level; b: Genus level)

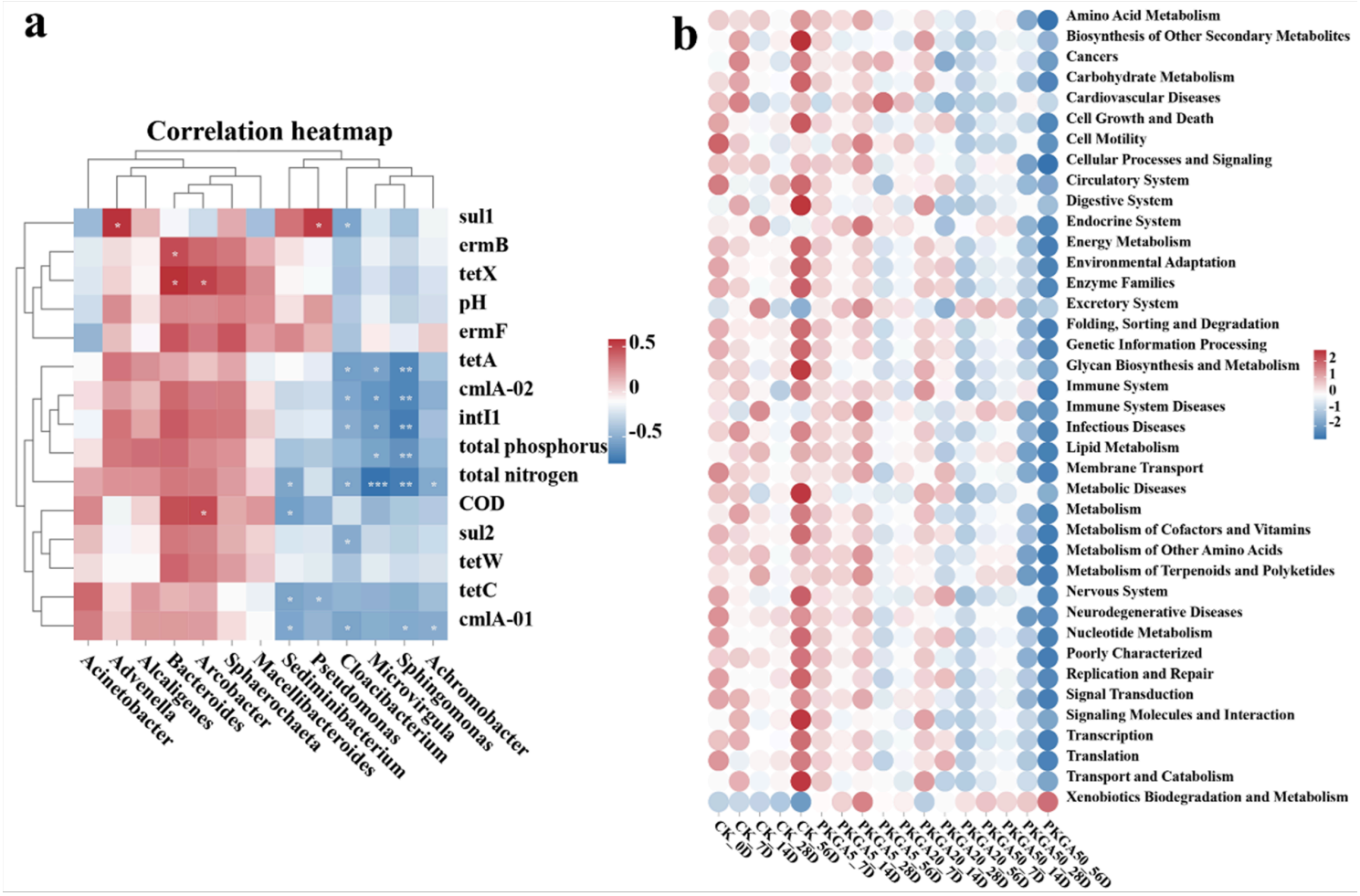


Figure 7

Correlation among genera, ARGs, MGEs, and environmental factors (a) and predicted microbial metabolic functions (b)

Supplementary Files

This is a list of supplementary files associated with this preprint. Click to download.

- SupportingInformation.docx
- SupplementaryTables.docx
- SupplementaryFigures.docx